Many-body localization in clean chains with long-range interactions

Chen Cheng *

Key Laboratory of Quantum Theory and Applications of MoE, Lanzhou Center for Theoretical Physics, and Key Laboratory of Theoretical Physics of Gansu Province, Lanzhou University, Lanzhou, Gansu 730000, China

(Received 18 June 2023; revised 9 August 2023; accepted 27 September 2023; published 9 October 2023)

Strong long-range interaction leads to localization in a closed quantum system without disorders. Employing the exact diagonalization method, I numerically investigate thermalization and many-body localization in translational invariant quantum chains with finite Coulomb interactions. In the computational basis, excluding all trivial degeneracies, the interaction-induced localization is well demonstrated in aspects of level statistics, eigenstate expectation values, and Anderson localization on graphs constructed of many-body bases. The nature of localization for generic eigenstates is attributed to the quasidisorder from the power-law interactions, and the full localization in the Hilbert space is similar to that in the disorder case. However, due to real-space symmetries, the long-time dynamics is dominated by the degenerated eigenstates and eventually reaches homogeneity in real space. On the other hand, the entanglement entropy exhibits size dependence beyond the area law for the same reason, even deep in the localized state, indicating an incomplete localization in real space.

DOI: 10.1103/PhysRevB.108.155113

I. INTRODUCTION

The dynamics of isolated quantum many-body systems has been extensively studied in recent years, and a new paradigm focus on the out-of-equilibrium quantum phase transition has been established. In the interacting and nonintegrable setting, the unitary dynamics of a generic quantum system drives the system to the thermalized state, and this ergodic phase is characterized by the eigenstate thermalization hypothesis (ETH) [1–4]. In contrast, the system affected by sufficient disorders features many-body localization (MBL) and fails to thermalize. Its long-time evolution partially preserves the encoded information of the initial state [5,6]. Thermalization and MBL in the presence of disorder can be characterized by essential differences in aspects such as level statistics [7–9] and entanglement entropy of eigenstates and its real-time spread behavior [10–12], and they have attracted many experimental probes in various platforms [13–21].

Although MBL is mainly studied in disordered systems as it has its roots in the nonergodicity of the well-known disorder-induced Anderson localization for noniteracting particles [22,23], disorder-free MBL and other ETH breakdown scenarios in the absence of disorder have attracted increasing interest [24–40]. The related studies bring attention to new issues like Stark MBL [26–28], quantum many-body scars [40–42], and Hilbert space fragmentation [33–35,39,40,43] and involve systems with conserved dipolar momentum [39], pairing hoppings [34,38], and strong constraints [44,45], to name a few. Specifically, the one-dimensional system with short-range interactions can be projected to a dynamically constrained model in the strongly interacting limit, where its Hilbert space fragments into an exponential number of disconnected sectors [45,46]. The real-time dynamics in different sectors can be qualitatively different, and some sectors feature complete localization in the presence of any finite disorders [45].

In parallel, the effect of long-range couplings in the context of thermalization and localization attracts interest in many aspects [47–70]. While both long-range interaction and hopping are generally believed to allow far-distance quantum correlations and to build up faster thermalization [48–51], it is reported that long-range couplings can lead to anomalous algebraic localization [52,53] and stabilize Stark MBL [64]. The logarithmic growth of the entanglement entropy over time, known as a unique characteristic of many-body localization, is also found in a noninteracting system with long-range hoppings [47]. Considering the cavity systems, the cavity-mediated global couplings not only allow the coexistence of MBL and long-range interactions [65,66] but also can lead to an inverted mobility edge [66].

Moreover, the possibility of disorder-free localization induced by long-range interactions has been proposed by recent studies [30–33,67,68]. Adopting the self-consistent mean-field theory, the authors in Ref. [67] propose that the long-range interaction can enhance localization and lower the critical disorder. If the interactions are sufficiently long-range, the system is always many-body localized even in the absence of disorder. From the numerical side, Ref. [31] explicitly demonstrates disorder-free localization in the presence of dipolar interactions, where the real-time evolution in this disorder-free MBL phase features abnormal two-stage dynamics. It has MBL-like behavior in a considerable time range but eventually thermalizes in the long-time limit. While the localization nature is due to Hilbert space fragmentation via strong interactions, the final thermalization is attributed to higher-order virtual excursions between fragmented Hilbert sections.

The dynamics with the coexistence of localization and thermalization nature in the clean long-range-interacted system is

*chengchen@lzu.edu.cn

beyond the picture of disorder-induced MBL. In this work, I revisit the disorder-free localization induced by long-range interactions and aim to understand better this incomplete MBL phenomenon. The interest in long-range-interacted systems also relies on the widely existing power-law interactions between particles in nature and the experimental developments simulating long-range interactions in platforms of ultracold polar molecules [71,72], trapped ions [73,74], and Rydberg gases [75].

II. MODEL AND NUMERICAL METHOD

The present work focuses on a one-dimensional bosonic Hubbard Hamiltonian with power-law interactions:

$$\hat{\mathcal{H}} = -t \sum_{\langle ij \rangle} \left(\hat{b}_i^\dagger \hat{b}_j + \text{H.c.} \right) + V \sum_{i<j} R_{i,j}^{-\beta} \hat{n}_i \hat{n}_j, \tag{1}$$

where $\hat{b}_i^\dagger$ ($\hat{b}_i$) is the hard-core bosonic creation (annihilation) operator at site i, $\hat{n}_i = \hat{b}_i^\dagger \hat{b}_i$ is the density operator, and $R_{i,j}$ denotes the distance between sites i and j in the system with size L. The strong long-range interaction leads to a Mott-insulating ground state of Eq. (1) and supports interesting ground-state physics when both charge and spin degrees of freedom are considered [76] or in higher dimensions [77,78]. The decay ratio β also affects the quench dynamics and the dynamical critical behavior in the transverse-field Ising chain [79,80]. Regarding the context of the ETH and its breakdown, it has recently been reported that sufficient dipole interactions result in Hilbert space fragmentation and MBL [31].

I consider the Coulomb interaction ($\beta = 1$), which is longer ranged than the dipole form and eliminates the multiband structure at relatively large V in the density of states (DOS) to have better level statistics. The Hamiltonian (1) conserves the total particle number $N = \langle \hat{N} \rangle = \sum_i \langle \hat{n}_i \rangle$, and the present work is restricted to the largest sector with half-filling $N = L/2$. The periodic boundary conditions are adopted to minimize the boundary effect. To rule out all trivial degeneracies and reduce the computational cost of the full exact diagonalization, the Hamiltonian matrix is constructed in basis $|s\rangle$, preserving the following symmetries as [81]

$$\hat{N}\hat{T}\hat{P}\hat{Z}|s\rangle = N e^{ik} pz |s\rangle. \tag{2}$$

Here $\hat{T}$ is the momentum operator, $k = 2m\pi/L$ ($m = -L/2, \ldots, 0, \ldots, L/2$) is the momentum, $\hat{P}$ ($\hat{Z}$) represents the reflection (particle-hole inversion) operator, and $p = \pm 1$ ($z = \pm 1$) is the corresponding parity. The Hilbert space dimension $\mathcal{N}$ is of the order of $\propto 2^L/(L \times L \times 2 \times 2)$, which is about 10^5 for the largest system size, $L = 26$, investigated. As a comparison, the paper also computes eigenstates in a basis with only conserved N and real-time evolution of the product states in Secs. III C and III D, with maximum size $L = 18$. For all numerical results, $t = 1$ is set as the energy scale.

III. RESULTS

While the disorder-free ETH breakdown due to sufficient long-range interactions has been investigated in the frame of Hilbert space fragmentation in previous studies [31,32], the present work aims to understand the phenomenon in an alternative aspect in which the Coulomb interaction can effectively introduce quasidisorders. Therefore, the numerical results are presented in a rather standard way of dealing with disordered localization problems. Specifically, Sec. III A characterizes thermalization and MBL using level statistics and eigenstate expectation values, and Sec. III B considers MBL to be a generalized Anderson localization problem. The full localization in Hilbert space is further confirmed by real-time dynamics in Sec. III C. In Sec. III D, I investigate the entanglement entropy and demonstrate that the generic eigenstate is not fully localized in real space.

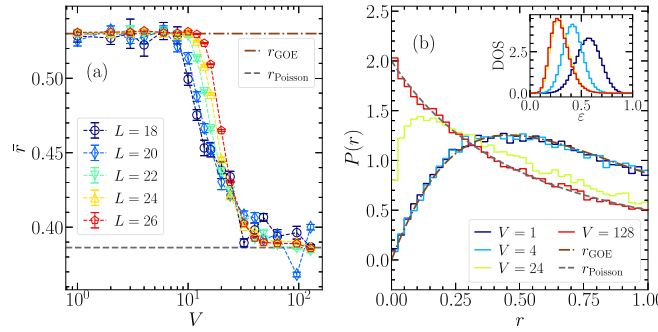

FIG. 1. (a) The mean ratio of adjacent gaps $\bar{r}$ versus interaction strength V for different system sizes L. Here the mean value and error are from the average over eight sectors with conserved momenta ($k = 0$ and $\pi/2$) and parities ($p \pm 1, z \pm 1$); within each sector, I consider energy levels in the middle half of the spectrum. (b) The distribution $P(r)$ for $L = 26$ and different values of V in the sector $\{k = 0, p = z = 1\}$. The inset displays the density of state in the same sector as a function of energy density $\varepsilon = (E - E_{\text{min}})/(E_{\text{max}} - E_{\text{min}})$.

A. Level statistics and thermalization predictions

Thermalization and localization are generally related to the ergodic and nonergodic regimes, which can be characterized by the spectrum structure and specifically quantified using the ratio of adjacent gaps [7–9], $r_\alpha \equiv \min(\delta_{\alpha+1}, \delta_\alpha)/\max(\delta_{\alpha+1}, \delta_\alpha)$, where $\delta_\alpha = E_\alpha - E_{\alpha-1}$ is the gap between adjacent energy levels and E_α is the αth eigenenergy. As displayed in Fig. 1(a), the average $\bar{r}$ agrees with the value predicted by the Gaussian orthogonal ensemble (GOE) at small interactions, indicating the ergodic phase in this region. At large V values, $\bar{r}$ approaches the value that obeys the Poisson distribution and shows localization characteristics. The results from different system sizes suggest the possibility of an ergodic-nonergodic transition as the jump of $\bar{r}$ becomes sharper as L increases.

The ergodic and nonergodic behaviors are further confirmed by the explicit distribution of r for several typical interactions at the largest $L = 26$, as shown in Fig. 1(b). The DOS in the inset Fig. 1(b) significantly differs at different V values; therefore, I take the average over the middle half of the spectrum to capture the physics at the infinite temperature instead of focusing on the fixed energy density. The continuous band manifests no obvious spectrum fragmentation at a large interaction, $V = 128$, which differs from the short-range and dipole interaction cases. The results in Fig. 1, which manifest the change of level statistics from ergodic to

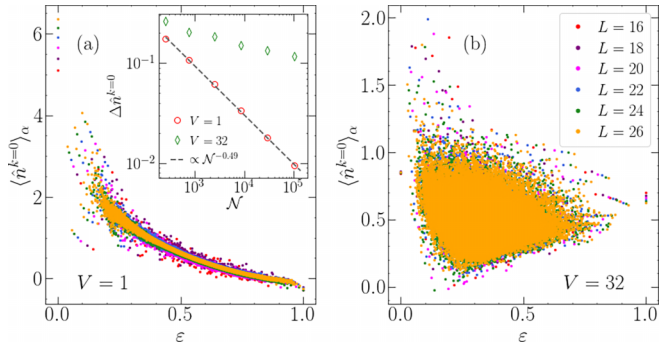

FIG. 2. Eigenstate expectation values $\langle \hat{n}^{k=0} \rangle_\alpha$ for (a) $V = 1$ and (b) $V = 32$ and different L values. The inset of panel (a) shows the fluctuations of consecutive eigenstate expectation values $\Delta n^{k=0}$ as a function of the Hilbert space dimension $\mathcal{N}$, where the dashed line displays the fitting to $\mathcal{N}^\gamma$ with $\gamma = -0.49$. Here the results correspond to the sector $\{k = 0,\ p = z = 1\}$.

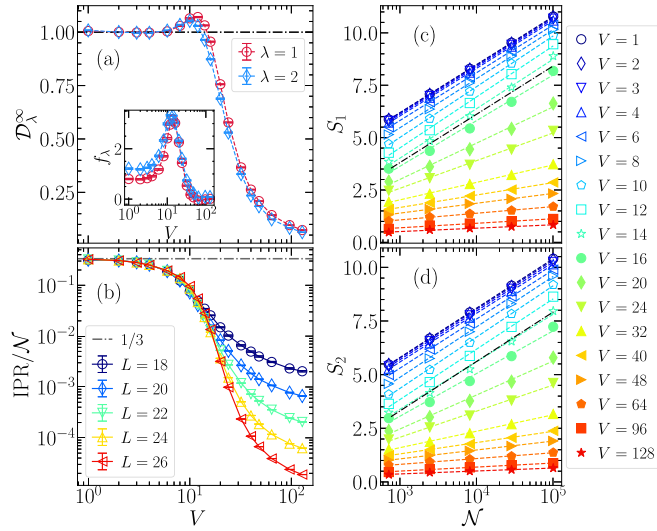

FIG. 3. (a) The multifractal dimension $\mathcal{D}_\lambda^\infty$ as a function of V, and the fitting parameter f_λ in the inset. (b) IPR/$\mathcal{N}$ as a function of V, where the horizontal line marks 1/3 from the ETH prediction. In panels (a) and (b), the mean value and error are from the average over eight sectors with conserved momenta k $(0, \pi/2)$ and parities p (± 1) and z (± 1). Panels (c) and (d) display the linear fitting $\mathcal{D}_\lambda(\mathcal{N}) = \mathcal{D}_\lambda^\infty - f_\lambda$ for S_1 and S_2, respectively. In panels (c) and (d), the data are from the sector $\{k = 0,\ p = z = 1\}$, and the black dashed line has a slope of 1.

nonergodic behavior in the full spectrum, are not simply predicted in the frame of strong-constraint-induced Hilbert space fragmentation. Note that in the limit $V \to \infty$, it is obvious that the eigenenergies approach the spectrum of the basis (2) with banded DOS and massive degeneracies, which is not the interest of the present work.

In the thermalized phase, the ETH predicts that the eigenstate expectation value of a generic few-body operator is a smooth function of energy [1–4]. On the contrary, in the MBL phase, the physical quantity is discontinuous even for eigenstates with very close energies. We verify the ergodicity of the system along this line by examining the zero momentum occupancy $\hat{n}^{k=0} = \frac{1}{L}\sum_{i,j} \hat{b}_i^\dagger \hat{b}_j$ as well as the corresponding eigenstate-to-eigenstate fluctuation $\Delta \hat{n}^{k=0} \equiv |\langle \hat{n}^{k=0} \rangle_\alpha - \langle \hat{n}^{k=0} \rangle_{\alpha+1}|$, where $\langle \rangle_\alpha$ denotes the expectation value of the eigenstate $|\alpha\rangle$. As displayed in Fig. 2(a), for the small $V = 1$, the possessed region of $\langle \hat{n}^{k=0} \rangle$ becomes narrower as the system size increases, which implies a smooth function of energy in the thermodynamic limit. In contrast, the same quantity in the MBL phase ($V = 32$) in Fig. 2(b) shows little system size dependency. In the inset of Fig. 2(a), there is a clear power-law behavior of the $\Delta \hat{n}^{k=0}$ as a function of Hilbert space dimension $\mathcal{N}$ in the thermal phase, where the fitting exponent -0.49 is in consistence with the $\mathcal{N}^{-1/2}$ behavior predicted by ETH analysis [82].

B. Anderson transition in random graphs

Anderson localization of single-particle orbitals is known to display multifractality at criticality [23]. Recent studies have observed a more generic Hilbert space multifractality in interacting systems and employed it to describe thermal-MBL transitions [83–87]. Rewriting the Hamiltonian (1) in the computational basis $|s\rangle$ [see Eq. (2)] as

$$\mathcal{H} = \sum_s \mu_s |s\rangle\langle s| + \sum_{s \neq s'} t_{ss'} |s\rangle\langle s'| \tag{3}$$

shows that MBL degenerates to a generalized Anderson localization problem, and the many-body bases $|s\rangle$ can be considered as complex Anderson orbitals. For the arbitrary many-body wave function $|\Psi\rangle = \sum_s \psi_s |s\rangle$, the interest related to multifractality lies in the mth participation entropy defined as

$$S_\lambda = \frac{1}{1-\lambda} \ln \left(\sum_{s=1}^{\mathcal{N}} |\psi_s|^{2\lambda} \right). \tag{4}$$

Specifically, $S_1 = -\sum_s |\psi_s|^2 \ln |\psi_s|^2$ is the Shannon entropy, and S_2 is the logarithm of the inverse participation ratio (IPR) [88] defined as $\mathrm{IPR} = 1/\sum_s |\psi_s|^4$. For a finite system with Hilbert space dimension $\mathcal{N}$, the λ-dependent fractal dimension $\mathcal{D}_\lambda$ measures the ergodic fraction of the Hilbert space, with $S_\lambda(\mathcal{N}) = \mathcal{D}(\mathcal{N}) \ln \mathcal{N}$. The asymptotic scaling approaching the infinite dimension follows the form $\mathcal{D}_\lambda(\mathcal{N}) = \mathcal{D}_\lambda^\infty - f_\lambda$ with a nonuniversal constant f_λ [83]; therefore, one can extract $\mathcal{D}_\lambda^\infty$ by the linear fitting $S_\lambda(\mathcal{N}) = \mathcal{D}_\lambda^\infty \ln \mathcal{N} - f_\lambda$.

As displayed in Fig. 3(a), $\mathcal{D}_\lambda^\infty$ as a function of interaction well demonstrates the trend of a dynamic transition: at small V values, $\mathcal{D}_\lambda^\infty = 1$ indicates fully ergodicity in the thermal phase; at larger interactions, $\mathcal{D}_\lambda^\infty < 1$ shows the multifractal behavior in the localized phase. The sharp peak of the fitting parameter f_λ also implies a possible transition point. Figures 3(c) and 3(d) explicitly display the fittings of S_1 and S_2, in the sector $\{k = 0,\ p = z = 1\}$ as an example, where both results suggest a critical interaction around $V = 14$ depicted by the black dash-dotted line with a slope of 1. The ergodicity breakdown is also demonstrated in Fig. 3(b) by displaying IPR/$\mathcal{N}$ for different system sizes and interactions. In the thermal region, IPR/$\mathcal{N}$ is almost independent of L, and the value agrees with the GOE prediction $\mathrm{IPR} = \mathcal{N}/3$ at very small interactions. In the localized region, IPR/$\mathcal{N}$ decays rapidly as L increases.

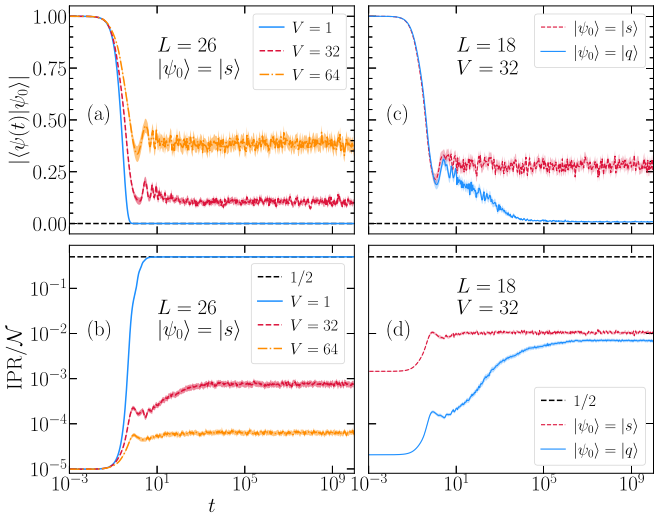

FIG. 4. Real-time evolution of (a) fidelity $|\langle\psi(t)|\psi(0)\rangle|$ and (b) IPR/$\mathcal{N}$ starting from the initial state $|s\rangle$ and maintaining all symmetries in the sector $\{k = 0,\ p = z = 1\}$, for $L = 26$ and different V values). Panels (c) and (d) compare the evolution from the product state $|q\rangle$ and the corresponding symmetric states $|s\rangle$. The evolution has been averaged over 64 random initial states in the middle half of the initial state spectrum.

The origin of this disorder-free localization can be understood in the aspect of a generalized Anderson localization problem with quasidisorders (3). In the many-body basis $|s\rangle$, the diagonal element $\mu_s = \langle s|\sum_R R^{-1}\hat{n}_R|s\rangle$ has a form similar to that of the disorder-induced MBL with $\mu_s^{\rm dis} = \langle s|\sum_i h_i\hat{n}_i|s\rangle$. Here R ($\hat{n}_R$) is the distance (density-density correlation operator) in the translational invariant basis, and h_i is the random on-site potential in the disordered case. In both forms, each diagonal element counts a summation of $\propto L$ different values and further provides $\propto \mathcal{N}$ possibilities for all diagonal elements of the Hamiltonian matrix in the many-body basis. In most studies on the disorder-induced MBL, h_i is uniformly distributed. However, in the clean case with Coulomb interactions, R^{-1} is discrete and decreases as a power law. This difference can lead to different features, such as the behavior of the fitting parameter f_λ. In the present work, f_λ is always positive and approaches zero deep in the MBL region, which differs from the disorder-induced thermal-MBL transition where the fitting parameter changes its sign at the critical point [84]. On the other hand, S_λ versus $\mathcal{N}$ shows nice linear behaviors for all V and L values used, which also differs from the disordered case.

C. Real-time dynamics

Localization in Hilbert space can be further confirmed by checking the real-time dynamics starting from a random state in the computational basis $|s\rangle$. In Fig. 4(a), the time-evolved fidelity $|\langle\psi(t)|\psi(0)\rangle|$ decays rapidly to zero for $V = 1$, agreeing with the fact that the dynamical return probability of a single site in the Hilbert space is infinitesimal in the chaotic system. In contrast, the Hilbert space cannot be fully visited in the localized phase, and the fidelity keeps a finite value at large interactions ($V = 32$ and 64). Unlike the two-step dynamics for the homogeneity parameter observed in Ref. [31], this high overlap with the initial state shows no indication for further decay, at least at the longest time (above 10^{10}) explored in this work. The evolution of IPR features similar dynamics. As displayed in Fig. 4(b), IPR/$\mathcal{N}$ approaches zero in a relatively short time in the thermal phase, but fluctuates around small values in the localized state. Here all the real-time evolution is averaged over 64 randomly initial states in the middle half of the spectrum to mimic the same physics with static quantities such as the level statistics [89].

Based on the above analysis on level statistics, eigenstate expectation values, Anderson localization in a many-body Hilbert space, and real-time dynamics of fidelity and the IPR, increasing Coulomb interaction leads to a full localization in the Hilbert space spanned by the basis $|s\rangle$, which is very similar to the disorder-induced localization. Next, to better understand the two-stage dynamics with the eventual thermalization of specific product states in boson chains with dipole interactions [31], I reinvestigate the localized phase in the basis of the product state $|q\rangle$, which conserves only the total particle N. Using possible combinations of trivial symmetries to an arbitrary product state, one retrieves the state $|s\rangle$ [90],

$$|s\rangle = 1/(\sqrt{2\times 2\times L})\sum_r (1+\hat{P})(1+\hat{Z})T^r|q\rangle, \qquad (5)$$

in the symmetric sector with $k = 0$ and $p = z = 1$. In the following, I compare the evolution of $|q\rangle$ and $|s\rangle$ in Eq. (5), and the latter is called the symmetric correspondence.

As shown in Fig. 4(c), the product state and its symmetric correspondence have almost the same short-time fidelity, which indicates the same short-relaxation behaviors. This is unsurprising since the evolution of an arbitrary $|q\rangle$ is equivalent under symmetry operations. At longer times, while the fidelity of $|s\rangle$ maintains the finite value, $|\langle\psi(t)|\psi(0)\rangle|$ for the product state features a slow logarithmic decay, providing clues of a final thermalization. However, as displayed in Fig. 4(d), although the IPR of the product state $|q\rangle$ continues to increase at a longer time range than the symmetric state $|s\rangle$, the two curves almost merge at the long-time limit and show the lack of ergodicity in the full Hilbert space. The different indications from fidelity and the IPR may arise from the degeneracy of the system in the product basis, in which case the evolution fully visits the subspace spanned by the degenerated eigenstates (with a dimension proportional to L) but not the full Hilbert space.

D. Entanglement entropy

While the above analysis suggests a full localization in the Hilbert space with quasidisorders, the evolution of a product state retrieves all real-space symmetries in the long-time limit and allows particle transport in real space. Based on this discrepancy, it is interesting to check further the real-space entanglement entropy of the eigenstates, which features the volume or area law in the standard thermal or MBL phase. The present work considers the most widely used half-chain entanglement entropy $S_{\rm ent} = {\rm Tr}\rho_A \ln \rho_A$, where $\rho_A = {\rm Tr}_B\rho$ is the reduced density matrix and ρ is the density matrix of the whole system, including two equally sized parts A and B.

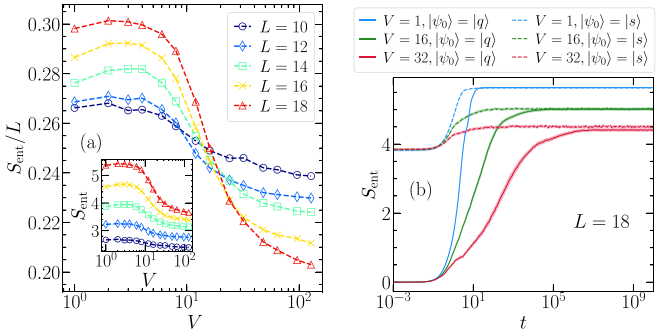

FIG. 5. (a) The entanglement entropy per site $S_{\rm ent}/L$ of the eigenstates versus V for different system sizes. The inset displays $S_{\rm ent}$. (b) Real-time evolution of $S_{\rm ent}$ for $L = 18$ and three typical V values, compared between the evolution from the product state $|q\rangle$ and the corresponding symmetric states $|s\rangle$. The choice of initial states is the same as that in Fig. 4.

In the inset of Fig. 5(a), for the system sizes investigated, $S_{\rm ent}$ increases as L increases, even in the localized state with large interactions. Furthermore, by checking the entanglement entropy per site, one observes a possible transition implied by the crossings of $S_{\rm ent}/L$ versus V for different system sizes. Regardless that one cannot rule out the finite size effect, the current data for system sizes up to $L = 18$ show an entanglement entropy behavior beyond volume law in the thermal phase and between area and volume law at large interactions. Although it is hard to properly extrapolate $S_{\rm ent}$ to the thermodynamic limit with the current results, one can roughly estimate the minimum size dependence of a generic translational invariant state as $S_{\rm ent} \propto \ln L$, which gives a lower bound of the eigenstate entanglement in the localized phase. This logarithmic size dependence reminds us of the gapless ground state with long-range order and finite transport [91,92], which is not localized in real space.

The evolution of entanglement entropy is displayed in Fig. 5(b). The symmetric initial state $|s\rangle$ is already highly entangled in real space, and the evolution starting from which reaches the long-time limit in a relatively short time. For the nonentangled product states, the quench dynamics are different in different phases: $S_{\rm ent}$ rapidly saturates in the thermal phase ($V = 1$) but has a long-time slow growth in the localized phase ($V = 32$). Here the evolution starting from a product $|q\rangle$ may have a short-time relaxation nature similar to that of its symmetric correspondence $|s\rangle$, mostly contributed by the direct hoppings of the Hamiltonian (1). At long times, higher-order processes, especially for those between product states generated by symmetry operators from the same $|q\rangle$, dominate the dynamics and eventually reach ergodicity in a subset of the Hilbert space. This subspace, which is determined by the long-time evolution of the corresponding symmetric states $|s\rangle$, can be a small fraction of the full Hilbert space at large interactions.

IV. CONCLUSION AND DISCUSSION

The strong Coulomb interaction in the one-dimensional bosonic chains leads to unconventional localization without disorders. In the computational basis ruling out all trivial symmetries, interaction-induced localization is nicely characterized by the level statistics, the eigenstate expectation values, the multifractality in the Hilbert space, and the time evolution of fidelity and the IPR. Here the nature of localization is attributed to the quasidisorder provided by the Coulomb interactions, and the full localization for generic eigenstates is well-defined in the Hilbert space without borrowing the concept of Hilbert space fragmentation. It is worth noting that the interaction is relatively strong but still finite with a nonbanded DOS, away from the infinite interacting limit.

However, due to real-space symmetries and the consequent degeneracy, the real-time dynamics of a product state in the localized phase exhibits two different timescales. After a short-time relaxation on account of the direct hopping term, the higher-order processes connecting all equivalent product states under symmetry operations dominate the long-time behaviors, ultimately merging the evolution of the corresponding symmetric state. In this procedure, the evolution retrieves all trivial symmetries and allows transport in real space. In this sense, the localization is not complete in real space. For the same reason, the entanglement entropy of the localized eigenstate with the real-space symmetries has a size dependence beyond the area law. This long-range interaction-induced localization in clean chains is beyond the picture of the l bits [93,94] of the disorder-induced MBL and deserves further investigation.

It is also interesting to reconsider the present results along the line of Hilbert space fragmentation, and all results suggest that the symmetric state $|s\rangle$ marks an individual fragmented section in the Hilbert space spanned by the product states $|q\rangle$. For the clean chains with long-range interactions, one observes full ergodicity within the fragmented section but ergodicity breaking between sections $|s\rangle$. This differs from the Stark MBL, where the system features ergodicity breaking inside the dipolar-momentum-conserved fragmented sections [95]. Again, I attribute this long-time ergodicity to real-space symmetries and degeneracy. Any perturbation that breaks the real-space symmetries, such as disorders or a linear potential, would lead to full MBL. The former has been confirmed in the dipolar interacting systems [31].

ACKNOWLEDGMENTS

This work is supported by the National Natural Science Foundation of China (Grants No. 12174167, No. 11904145, and No. 12247101), the 111 Project under Grant No. 20063, and the Fundamental Research Funds for the Central Universities.

[1] J. M. Deutsch, Quantum statistical mechanics in a closed system, Phys. Rev. A **43**, 2046 (1991).
[2] M. Srednicki, Chaos and quantum thermalization, Phys. Rev. E **50**, 888 (1994).
[3] M. Rigol, V. Dunjko, and M. Olshanii, Thermalization and its mechanism for generic isolated quantum systems, Nature (London) **452**, 854 (2008).

[4] L. D'Alessio, Y. Kafri, A. Polkovnikov, and M. Rigol, From quantum chaos and eigenstate thermalization to statistical mechanics and thermodynamics, Adv. Phys. **65**, 239 (2016).

[5] R. Nandkishore and D. A. Huse, Many-body localization and thermalization in quantum statistical mechanics, Annu. Rev. Condens. Matter Phys. **6**, 15 (2015).

[6] D. A. Abanin, E. Altman, I. Bloch, and M. Serbyn, Colloquium: Many-body localization, thermalization, and entanglement, Rev. Mod. Phys. **91**, 021001 (2019).

[7] V. Oganesyan and D. A. Huse, Localization of interacting fermions at high temperature, Phys. Rev. B **75**, 155111 (2007).

[8] A. Pal and D. A. Huse, Many-body localization phase transition, Phys. Rev. B **82**, 174411 (2010).

[9] Y. Y. Atas, E. Bogomolny, O. Giraud, and G. Roux, Distribution of the ratio of consecutive level spacings in random matrix ensembles, Phys. Rev. Lett. **110**, 084101 (2013).

[10] M. Žnidarič, T. Prosen, and P. Prelovšek, Many-body localization in the Heisenberg XXZ magnet in a random field, Phys. Rev. B **77**, 064426 (2008).

[11] J. H. Bardarson, F. Pollmann, and J. E. Moore, Unbounded growth of entanglement in models of many-body localization, Phys. Rev. Lett. **109**, 017202 (2012).

[12] M. Serbyn, Z. Papić, and D. A. Abanin, Universal slow growth of entanglement in interacting strongly disordered systems, Phys. Rev. Lett. **110**, 260601 (2013).

[13] M. Schreiber, S. S. Hodgman, P. Bordia, H. P. Lüschen, M. H. Fischer, R. Vosk, E. Altman, U. Schneider, and I. Bloch, Observation of many-body localization of interacting fermions in a quasirandom optical lattice, Science **349**, 842 (2015).

[14] J.-Y. Choi, S. Hild, J. Zeiher, P. Schauß, A. Rubio-Abadal, T. Yefsah, V. Khemani, D. A. Huse, I. Bloch, and C. Gross, Exploring the many-body localization transition in two dimensions, Science **352**, 1547 (2016).

[15] J. Smith, A. Lee, P. Richerme, B. Neyenhuis, P. W. Hess, P. Hauke, M. Heyl, D. A. Huse, and C. Monroe, Many-body localization in a quantum simulator with programmable random disorder, Nat. Phys. **12**, 907 (2016).

[16] H. P. Lüschen, P. Bordia, S. Scherg, F. Alet, E. Altman, U. Schneider, and I. Bloch, Observation of slow dynamics near the many-body localization transition in one-dimensional quasiperiodic systems, Phys. Rev. Lett. **119**, 260401 (2017).

[17] P. Roushan, C. Neill, J. Tangpanitanon, V. M. Bastidas, A. Megrant, R. Barends, Y. Chen, Z. Chen, B. Chiaro, A. Dunsworth, A. Fowler, B. Foxen, M. Giustina, E. Jeffrey, J. Kelly, E. Lucero, J. Mutus, M. Neeley, C. Quintana, D. Sank *et al.*, Spectroscopic signatures of localization with interacting photons in superconducting qubits, Science **358**, 1175 (2017).

[18] K. Xu, J.-J. Chen, Y. Zeng, Y.-R. Zhang, C. Song, W. Liu, Q. Guo, P. Zhang, D. Xu, H. Deng, K. Huang, H. Wang, X. Zhu, D. Zheng, and H. Fan, Emulating many-body localization with a superconducting quantum processor, Phys. Rev. Lett. **120**, 050507 (2018).

[19] K. X. Wei, C. Ramanathan, and P. Cappellaro, Exploring localization in nuclear spin chains, Phys. Rev. Lett. **120**, 070501 (2018).

[20] M. Rispoli, A. Lukin, R. Schittko, S. Kim, M. E. Tai, J. Léonard, and M. Greiner, Quantum critical behaviour at the many-body localization transition, Nature (London) **573**, 385 (2019).

[21] Q. Guo, C. Cheng, Z.-H. Sun, Z. Song, H. Li, Z. Wang, W. Ren, H. Dong, D. Zheng, Y.-R. Zhang, R. Mondaini, H. Fan, and H. Wang, Observation of energy-resolved many-body localization, Nat. Phys. **17**, 234 (2021).

[22] P. W. Anderson, Absence of diffusion in certain random lattices, Phys. Rev. **109**, 1492 (1958).

[23] F. Evers and A. D. Mirlin, Anderson transitions, Rev. Mod. Phys. **80**, 1355 (2008).

[24] A. Smith, J. Knolle, D. L. Kovrizhin, and R. Moessner, Disorder-free localization, Phys. Rev. Lett. **118**, 266601 (2017).

[25] M. Schiulaz, A. Silva, and M. Müller, Dynamics in many-body localized quantum systems without disorder, Phys. Rev. B **91**, 184202 (2015).

[26] M. Schulz, C. A. Hooley, R. Moessner, and F. Pollmann, Stark many-body localization, Phys. Rev. Lett. **122**, 040606 (2019).

[27] E. V. H. Doggen, I. V. Gornyi, and D. G. Polyakov, Stark many-body localization: Evidence for Hilbert-space shattering, Phys. Rev. B **103**, L100202 (2021).

[28] Q. Guo, C. Cheng, H. Li, S. Xu, P. Zhang, Z. Wang, C. Song, W. Liu, W. Ren, H. Dong, R. Mondaini, and H. Wang, Stark many-body localization on a superconducting quantum processor, Phys. Rev. Lett. **127**, 240502 (2021).

[29] W. Li, A. Dhar, X. Deng, K. Kasamatsu, L. Barbiero, and L. Santos, Disorderless quasi-localization of polar gases in one-dimensional lattices, Phys. Rev. Lett. **124**, 010404 (2020).

[30] L. Barbiero, C. Menotti, A. Recati, and L. Santos, Out-of-equilibrium states and quasi-many-body localization in polar lattice gases, Phys. Rev. B **92**, 180406(R) (2015).

[31] W.-H. Li, X. Deng, and L. Santos, Hilbert space shattering and disorder-free localization in polar lattice gases, Phys. Rev. Lett. **127**, 260601 (2021).

[32] H. Korbmacher, P. Sierant, W. Li, X. Deng, J. Zakrzewski, and L. Santos, Lattice control of nonergodicity in a polar lattice gas, Phys. Rev. A **107**, 013301 (2023).

[33] V. Khemani, M. Hermele, and R. Nandkishore, Localization from Hilbert space shattering: From theory to physical realizations, Phys. Rev. B **101**, 174204 (2020).

[34] L. Herviou, J. H. Bardarson, and N. Regnault, Many-body localization in a fragmented Hilbert space, Phys. Rev. B **103**, 134207 (2021).

[35] P. Frey, L. Hackl, and S. Rachel, Hilbert space fragmentation and interaction-induced localization in the extended Fermi-Hubbard model, Phys. Rev. B **106**, L220301 (2022).

[36] N. Chakraborty, M. Heyl, P. Karpov, and R. Moessner, Disorder-free localization transition in a two-dimensional lattice gauge theory, Phys. Rev. B **106**, L060308 (2022).

[37] S. Moudgalya, A. Prem, R. Nandkishore, N. Regnault, and B. A. Bernevig, Thermalization and its absence within Krylov subspaces of a constrained Hamiltonian, in *Memorial Volume for Shoucheng Zhang*, edited by B. Lian, C.-X. Liu, E. Demler, S. Kievelson, and X.-L. Qi (World Scientific, Singapore, 2021), Chap. 7, pp. 147–209.

[38] S. Moudgalya and O. I. Motrunich, Hilbert space fragmentation and commutant algebras, Phys. Rev. X **12**, 011050 (2022).

[39] P. Sala, T. Rakovszky, R. Verresen, M. Knap, and F. Pollmann, Ergodicity breaking arising from hilbert space fragmentation in dipole-conserving Hamiltonians, Phys. Rev. X **10**, 011047 (2020).

[40] S. Moudgalya, B. A. Bernevig, and N. Regnault, Quantum many-body scars and Hilbert space fragmentation: a review of exact results, Rep. Prog. Phys. **85**, 086501 (2022).

[41] C. J. Turner, A. A. Michailidis, D. A. Abanin, M. Serbyn, and Z. Papić, Weak ergodicity breaking from quantum many-body scars, Nat. Phys. **14**, 745 (2018).
[42] D. Bluvstein, A. Omran, H. Levine, A. Keesling, G. Semeghini, S. Ebadi, T. T. Wang, A. A. Michailidis, N. Maskara, W. W. Ho, S. Choi, M. Serbyn, M. Greiner, V. Vuletić, and M. D. Lukin, Controlling quantum many-body dynamics in driven rydberg atom arrays, Science **371**, 1355 (2021).
[43] B. Mukherjee, D. Banerjee, K. Sengupta, and A. Sen, Minimal model for Hilbert space fragmentation with local constraints, Phys. Rev. B **104**, 155117 (2021).
[44] R. M. Nandkishore and M. Hermele, Fractons, Annu. Rev. Condens. Matter Phys. **10**, 295 (2019).
[45] G. De Tomasi, D. Hetterich, P. Sala, and F. Pollmann, Dynamics of strongly interacting systems: From Fock-space fragmentation to many-body localization, Phys. Rev. B **100**, 214313 (2019).
[46] T. Rakovszky, P. Sala, R. Verresen, M. Knap, and F. Pollmann, Statistical localization: From strong fragmentation to strong edge modes, Phys. Rev. B **101**, 125126 (2020).
[47] R. Singh, R. Moessner, and D. Roy, Effect of long-range hopping and interactions on entanglement dynamics and many-body localization, Phys. Rev. B **95**, 094205 (2017).
[48] A. L. Burin, Many-body delocalization in a strongly disordered system with long-range interactions: Finite-size scaling, Phys. Rev. B **91**, 094202 (2015).
[49] K. S. Tikhonov and A. D. Mirlin, Many-body localization transition with power-law interactions: Statistics of eigenstates, Phys. Rev. B **97**, 214205 (2018).
[50] A. O. Maksymov and A. L. Burin, Many-body localization in spin chains with long-range transverse interactions: Scaling of critical disorder with system size, Phys. Rev. B **101**, 024201 (2020).
[51] D. S. Bhakuni and A. Sharma, Stability of electric field driven many-body localization in an interacting long-range hopping model, Phys. Rev. B **102**, 085133 (2020).
[52] X. Deng, V. E. Kravtsov, G. V. Shlyapnikov, and L. Santos, Duality in power-law localization in disordered one-dimensional systems, Phys. Rev. Lett. **120**, 110602 (2018).
[53] X. Deng, S. Ray, S. Sinha, G. V. Shlyapnikov, and L. Santos, One-dimensional quasicrystals with power-law hopping, Phys. Rev. Lett. **123**, 025301 (2019).
[54] X. Wei, C. Cheng, G. Xianlong, and R. Mondaini, Investigating many-body mobility edges in isolated quantum systems, Phys. Rev. B **99**, 165137 (2019).
[55] P. A. Nosov, I. M. Khaymovich, and V. E. Kravtsov, Correlation-induced localization, Phys. Rev. B **99**, 104203 (2019).
[56] P. A. Nosov and I. M. Khaymovich, Robustness of delocalization to the inclusion of soft constraints in long-range random models, Phys. Rev. B **99**, 224208 (2019).
[57] R. Modak and T. Nag, Many-body localization in a long-range model: Real-space renormalization-group study, Phys. Rev. E **101**, 052108 (2020).
[58] R. Modak and T. Nag, Many-body dynamics in long-range hopping models in the presence of correlated and uncorrelated disorder, Phys. Rev. Res. **2**, 012074(R) (2020).
[59] A. Lerose and S. Pappalardi, Origin of the slow growth of entanglement entropy in long-range interacting spin systems, Phys. Rev. Res. **2**, 012041(R) (2020).
[60] X. Deng, G. Masella, G. Pupillo, and L. Santos, Universal algebraic growth of entanglement entropy in many-body localized systems with power-law interactions, Phys. Rev. Lett. **125**, 010401 (2020).
[61] T. Kuwahara and K. Saito, Absence of fast scrambling in thermodynamically stable long-range interacting systems, Phys. Rev. Lett. **126**, 030604 (2021).
[62] D. D. Vu, K. Huang, X. Li, and S. Das Sarma, Fermionic many-body localization for random and quasiperiodic systems in the presence of short- and long-range interactions, Phys. Rev. Lett. **128**, 146601 (2022).
[63] A. Marie, D. P. Kooi, J. Grossi, M. Seidl, Z. H. Musslimani, K. J. H. Giesbertz, and P. Gori-Giorgi, Real-space Mott-Anderson electron localization with long-range interactions, Phys. Rev. Res. **4**, 043192 (2022).
[64] I. V. Lukin, Y. V. Slyusarenko, and A. G. Sotnikov, Many-body localization in a quantum gas with long-range interactions and linear external potential, Phys. Rev. B **105**, 184307 (2022).
[65] R.-C. Ge, S. R. Koshkaki, and M. H. Kolodrubetz, Cavity induced many-body localization, arXiv:2208.06898.
[66] S. R. Koshkaki and M. H. Kolodrubetz, Inverted many-body mobility edge in a central qudit problem, Phys. Rev. B **105**, L060303 (2022).
[67] S. Roy and D. E. Logan, Self-consistent theory of many-body localisation in a quantum spin chain with long-range interactions, SciPost Phys. **7**, 042 (2019).
[68] B. Pandey, E. Dagotto, and S. K. Pati, Quench dynamics of two-component dipolar fermions subject to a quasiperiodic potential, Phys. Rev. B **102**, 214302 (2020).
[69] R. Yousefjani and A. Bayat, Mobility edge in long-range interacting many-body localized systems, Phys. Rev. B **107**, 045108 (2023).
[70] K. Huang, D. D. Vu, X. Li, and S. Das Sarma, Incommensurate many-body localization in the presence of long-range hopping and single-particle mobility edge, Phys. Rev. B **107**, 035129 (2023).
[71] A. V. Gorshkov, S. R. Manmana, G. Chen, J. Ye, E. Demler, M. D. Lukin, and A. M. Rey, Tunable superfluidity and quantum magnetism with ultracold polar molecules, Phys. Rev. Lett. **107**, 115301 (2011).
[72] A. V. Gorshkov, S. R. Manmana, G. Chen, E. Demler, M. D. Lukin, and A. M. Rey, Quantum magnetism with polar alkali-metal dimers, Phys. Rev. A **84**, 033619 (2011).
[73] P. Richerme, Z.-X. Gong, A. Lee, C. Senko, J. Smith, M. Foss-Feig, S. Michalakis, A. V. Gorshkov, and C. Monroe, Non-local propagation of correlations in quantum systems with long-range interactions, Nature (London) **511**, 198 (2014).
[74] P. Jurcevic, B. P. Lanyon, P. Hauke, C. Hempel, P. Zoller, R. Blatt, and C. F. Roos, Quasiparticle engineering and entanglement propagation in a quantum many-body system, Nature (London) **511**, 202 (2014).
[75] H. Bernien, S. Schwartz, A. Keesling, H. Levine, A. Omran, H. Pichler, S. Choi, A. S. Zibrov, M. Endres, M. Greiner, V. Vuletić, and M. D. Lukin, Probing many-body dynamics on a 51-atom quantum simulator, Nature (London) **551**, 579 (2017).
[76] C. Cheng, B.-B. Mao, F.-Z. Chen, and H.-G. Luo, Phase diagram of the one-dimensional t-J model with long-range dipolar interactions, Europhys. Lett. **110**, 37002 (2015).
[77] L. Yang, P. Weinberg, and A. E. Feiguin, Topological to magnetically ordered quantum phase transition in antiferromagnetic

spin ladders with long-range interactions, SciPost Phys. **13**, 060 (2022).
[78] Z. Gong, T. Guaita, and J. I. Cirac, Long-range free fermions: Lieb-Robinson bound, clustering properties, and topological phases, Phys. Rev. Lett. **130**, 070401 (2023).
[79] J. C. Halimeh, V. Zauner-Stauber, I. P. McCulloch, I. de Vega, U. Schollwöck, and M. Kastner, Prethermalization and persistent order in the absence of a thermal phase transition, Phys. Rev. B **95**, 024302 (2017).
[80] J. C. Halimeh, M. Van Damme, L. Guo, J. Lang, and P. Hauke, Dynamical phase transitions in quantum spin models with antiferromagnetic long-range interactions, Phys. Rev. B **104**, 115133 (2021).
[81] A. W. Sandvik, Computational studies of quantum spin systems, AIP Conf. Proc. **1297**, 135 (2010).
[82] W. Beugeling, R. Moessner, and M. Haque, Finite-size scaling of eigenstate thermalization, Phys. Rev. E **89**, 042112 (2014).
[83] A. Bäcker, M. Haque, and I. M. Khaymovich, Multifractal dimensions for random matrices, chaotic quantum maps, and many-body systems, Phys. Rev. E **100**, 032117 (2019).
[84] N. Macé, F. Alet, and N. Laflorencie, Multifractal scalings across the many-body localization transition, Phys. Rev. Lett. **123**, 180601 (2019).
[85] F. Pietracaprina and N. Laflorencie, Hilbert-space fragmentation, multifractality, and many-body localization, Ann. Phys. **435**, 168502 (2021).
[86] Y. Wang, C. Cheng, X.-J. Liu, and D. Yu, Many-body critical phase: Extended and nonthermal, Phys. Rev. Lett. **126**, 080602 (2021).
[87] J. Sutradhar, S. Ghosh, S. Roy, D. E. Logan, S. Mukerjee, and S. Banerjee, Scaling of the Fock-space propagator and multifractality across the many-body localization transition, Phys. Rev. B **106**, 054203 (2022).
[88] W. Visscher, Localization of electron wave functions in disordered systems, J. Non-Cryst. Solids **8-10**, 477 (1972).
[89] By the averaging over many random initial states, we neglect the influence of possible low-measure (or even measure-zero) special initial states, like the one-mover blocks in Ref. [45] and the localization plateau for the special initial state in Ref. [31]. This work focuses on the general strong ETH break scenario, but not the Hilbert space fragmentation or special state localization such as quantum scars.
[90] Although the present does not aim to inspire the immediate experiment at the current stage, I would like to address that the entangled initial state can be potentially prepared in experiments in the frame of quantum computing [96–98]. On the other hand, the periodic chain can be realized by superconducting qubits, such as the device in Ref. [21].
[91] P. Calabrese and J. Cardy, Entanglement entropy and quantum field theory, J. Stat. Mech. (2004) P06002.
[92] A. M. Läuchli and C. Kollath, Spreading of correlations and entanglement after a quench in the one-dimensional bose-hubbard model, J. Stat. Mech. (2008) P05018.
[93] J. Z. Imbrie, V. Ros, and A. Scardicchio, Local integrals of motion in many-body localized systems, Ann. Phys. **529**, 1600278 (2017).
[94] L. Rademaker, M. Ortuño, and A. M. Somoza, Many-body localization from the perspective of integrals of motion, Ann. Phys. **529**, 1600322 (2017).
[95] See Fig. S10 in the Supplemental Material of Ref. [28], where the Poisson distribution of level statistics is shown in the fragmented island.
[96] M. Neeley, R. C. Bialczak, M. Lenander, E. Lucero, M. Mariantoni, A. D. O'Connell, D. Sank, H. Wang, M. Weides, J. Wenner, Y. Yin, T. Yamamoto, A. N. Cleland, and J. M. Martinis, Generation of three-qubit entangled states using superconducting phase qubits, Nature (London) **467**, 570 (2010).
[97] A. Omran, H. Levine, A. Keesling, G. Semeghini, T. T. Wang, S. Ebadi, H. Bernien, A. S. Zibrov, H. Pichler, S. Choi, J. Cui, M. Rossignolo, P. Rembold, S. Montangero, T. Calarco, M. Endres, M. Greiner, V. Vuletić, and M. D. Lukin, Generation and manipulation of Schrödinger cat states in Rydberg atom arrays, Science **365**, 570 (2019).
[98] C. Song, K. Xu, H. Li, Y.-R. Zhang, X. Zhang, W. Liu, Q. Guo, Z. Wang, W. Ren, J. Hao, H. Feng, H. Fan, D. Zheng, D.-W. Wang, H. Wang, and S.-Y. Zhu, Generation of multicomponent atomic Schrödinger cat states of up to 20 qubits, Science **365**, 574 (2019).